Volume 69, Issue 3, 2025
Journal of Scientific Research
of
The Banaras Hindu University

Laser Raman Scanning and 3D Mapping of Pyrite Crystal in Carbonaceous Phyllite from Zawar Lead-Zinc Deposits, Rajasthan

Akansha Gupta and Dinesh Pandit*

Department of Geology, Institute of Science, Banaras Hindu University, Varanasi, Uttar Pradesh, India, *e-mail id: dpandit@hotmail.com

Abstract: **The Mochia-Magra mine is a significant carbonate-hosted lead-zinc orebody located in the Zawar Formation of the Middle Aravalli Supergroup. Pyrite occurs in the carbonaceous phyllite, the host rock of the Mochia-Magra mines, occur as a minor component of the ore assemblages in association with quartz and calcite. Petrographic studies reveals that the euhedral to subhedral pyrite crystals are frequently occurs, a characteristic perfectly developed external facet crystals, often associated in the carbonaceous phyllite. Pyrite and calcite phase show diagnostic Raman Shift ~383 cm^{-1} and ~1098 cm^{-1} ascribed to symmetric Ag stretching vibration mode of phase S-S and symmetric stretching (ν_1) vibration mode of the $(CO_3)^{2-}$ group, respectively. In this study, Laser Raman scanning, 2D and 3D mapping of euhedral pyrite crystal infer their inhomogeneous composition in the carbonaceous phyllite. Pyrite crystallizes from hydrothermal fluids with fluctuations in iron (Fe^{2+}) and sulphur (SO_4^{2-} or H_2S) concentrations in reducing environment, variation in temperature and pressure favour specific crystal growth conditions within carbonaceous phyllite. Origin of euhedral pyrite crystals accredited to specific geological conditions, possibly hydrothermal fluids that influenced chemical precipitation processes, in the Paleoproterozoic Zawar lead-zinc deposit. Inhomogeneities within a pyrite crystal can enhance geochemical analysis, helping to decipher the ore genesis and their role in lead-zinc metallogeny.**

Index Terms: **Laser Raman, Pyrite, Quartz, Calcite, Zawar Pb-Zn deposits.**

I. Introduction

The Laser Raman Micro Spectroscopy (LRMS) probe is an in-situ high-resolution imaging method (Raman, 1923; 1928; 1929; Raman and Krishnan, 1928) that combines Scanning Nearfield Optical Microscopy (SNOM), allowing for the acquisition of chemical and topographical information at the nanoscale (>100 nm) on surface characterization (Jones et al., 2019; Pandit, 2024). This integration overcomes the spatial resolution limitations of far-field Raman spectroscopy by using a sub-wavelength aperture on a cantilever to create an evanescent field that interacts with the sample, providing high-resolution confocal Raman images and chemical composition of mineral phases alongside surface topography (Aradi et al., 2023; Robinson et al., 2024). Overcomes, the diffraction limit of light in conventional Raman spectroscopy to achieve nanoscale resolution. This method provides label-free detection of chemical composition and in-situ characterization of mineral phases in rock samples (Kosek et al., 2023). The LRMS, non-destructive technique can identify a wide range of minerals, including those with similar chemical compositions but different crystal structures or polymorphs, by detecting their unique molecular vibrational modes (Rodgers, 1993; Bersani and Lottici, 2016). It offers high precision, requires little to no sample preparation, and can be performed in situ, even on tiny fluid inclusions within minerals (Misra et al., 2023). This method is widely used in materials science for analysing inorganic crystals, polymer films, and nano-carbon materials, as well as in semiconductor applications for identifying nanoscale defects and contamination.

Laser Raman characterization in Earth science involves using a laser to excite mineral samples, analysing the scattered light to reveal their molecular structure and chemical composition (McMillan, 1989; Nasdala and Schmidt, 2020). Applications include identifying minerals in ores, studying fluid and melt inclusions, characterizing planetary materials, and assessing geological processes. The LRMS technique characterizes natural minerals by analysing its vibrational modes, which are sensitive to its chemical composition, crystal orientation, and molecular configurations (Sharma et al., 2009). The technique is non-destructive, identifies individual grains, and can detect crystal

structure, such as sulphides or oxides or solid matrices, on the surface study of the mineral (Vandenabeele et al., 2013). The resulting Raman spectra exhibit variability due to factors like sample orientation, surface smoothness, and instrumental parameters, but can infer crystal morphology and help distinguish various minerals (Eberhardt et al., 2015).

The objective of this study focusses on characterization of mineral phases in the carbonaceous phyllite applying the LRMS technique with an excitation wavelength of 532 nm. In carbonaceous phyllite, occurrences of mineral phases helps to understand the origin of euhedral pyrite crystals in the orebody of the Mochia-Magra Mines in the Zawar deposit (Mookherjee, 1964; Roy, 1995; Sarkar and Banerjee, 2004).

II. Regional Geology

The Aravalli-Delhi Mobile Belt (ADMB), located in northwest India, is a geological region characterized by ancient supracrustal rocks of the Proterozoic Aravalli and Delhi Supergroups deposited over Banded Gneissic Complex (BGC) comprises of the Archean basement (Sharma, 2009; Biswal et al., 2022). This belt has experienced multiple phases of deformation and metamorphism, including the Aravalli orogeny (~2.5 to 1.7 Ga) and the subsequent Delhi orogeny (~2.0 to 0.7 Ga; Sharma, 2009; Roy and Puroit, 2015; Fareeduddin and Banerjee, 2020). The belt has undergone at least two significant Proterozoic orogenic events (Power and Patwardhan, 1984; Verma and Greiling, 1995). The Aravalli Supergroup typically show greenschist facies metamorphism, while the Delhi Supergroup rocks display metamorphism ranging from greenschist to granulite facies (Sharma, 2009). The Aravalli Supergroup is a sequence of Paleoproterozoic era (~2.5 to 2.0 Ga) metasedimentary and minor metavolcanic rocks that developed in basins above the older Archean BGC rocks (Roy, 1990). Key rock types include quartzites, phyllites, greywacks, and dolomitic limestones.

The Zawar lead-zinc deposits, located in Rajasthan, India, are hosted within carbonaceous phyllites, dolostones, dolomites and dolomitic limestones of the Paleoproterozoic Aravalli Supergroup (Deb and Sarkar, 1990; Bhattacharya and Bull, 2010). These deposits are strata-bound and have been subjected to later metamorphism and remobilization. The ore bodies are polymetallic sulphides, with key minerals including galena (lead) and sphalerite (zinc) in association with pyrite, chalcopyrite, and pyrrhotite (Mookherjee, 1964). The sulphide mineralization is strongly controlled by structural features, particularly the youngest set of shear planes and mineralized shear zones that developed concurrently with metallization (Singh, 1988; Roy, 1995). The lead-zinc mineralization occurs as cavity fillings and replacement veins within structural features like fault and fracture zones, and their development is closely linked to the youngest set of regional structural deformations (Talluri et al., 2000). The Zawar Pb-Zn deposits have undergone later tectonic and thermal metamorphism, which has led to the remobilization of sulphides and changes in mineralogy. The study focusses on the origin of sulphide ores in the Zawar Pb-Zn deposit and the specific crystal growth mechanism of pyrite in the phyllite host rock.

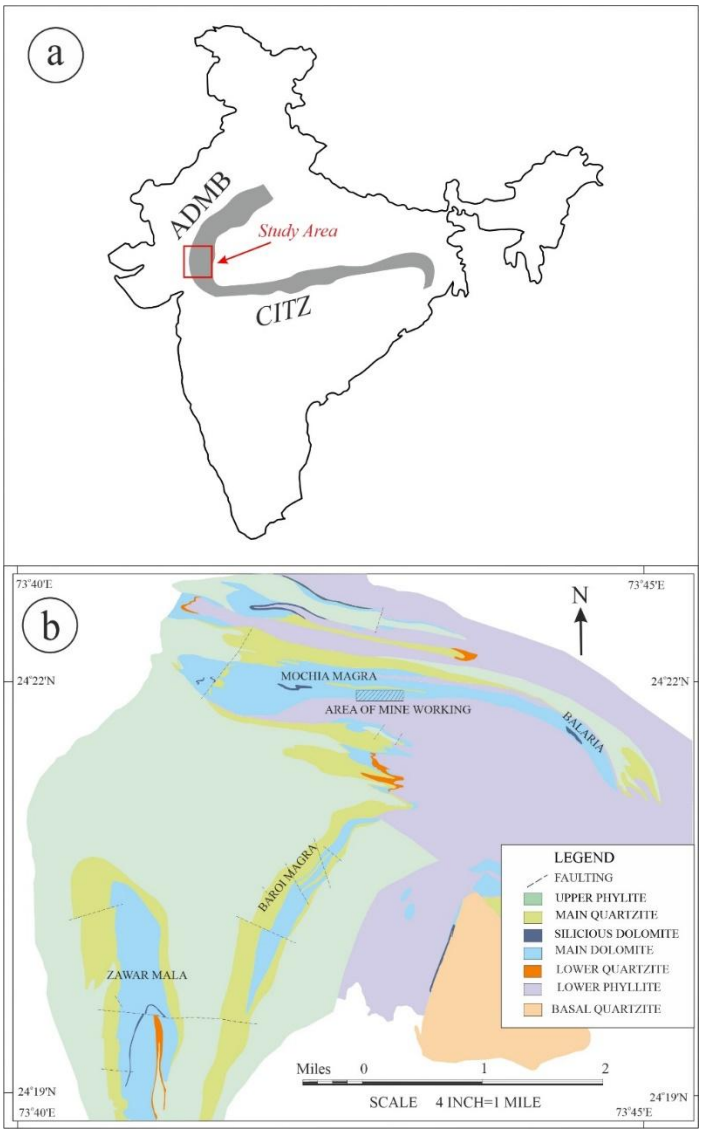

Fig. 1. (a) Outline of India map displays study area along the Aravalli Delhi Mobile Belt and (b) Geological map of Zawar Lead-Zinc Belt with locations of Zawarmala, Baroi and Mochia-Magra Mines in Udaipur district of Rajasthan (after Mookherjee, 1965; Chakrabarty, 1968).

III. Petrography

The ore mineralization in the ADMB, very of lead-zinc (Pb-Zn) is confined to the Zawar belt of the Mochia Formation. The Mochia Formation also known as Zawar Formation of the middle Aravalli Supergroup (Ramakrishnan and Vaidyanathan, 2008), consists of carbonaceous phyllite and carbonates that hosts important lead-zinc mineralization in Zawar deposit (Roy, 1995). The carbonaceous phyllite essentially consists of carbonates, chlorite and quartz, hosting principal sulphide minerals. The hand specimen exhibits silky sheen luster (Fig. 4), which is a defining

property of phyllite rock. The rock surface displays a reflective, shiny appearance and soapy to touch. This develops due to parallel alignment of fine-grained micaceous minerals such as chlorite, sericite, mica, etc. Deformation causes the parallel alignment of minerals. The presence of sulphide minerals is aligned along the cleavage planes. The host rock, phyllite is classified as low-grade metamorphic rock formed during regional metamorphism (Chakrabarty, 1967; Singh, 1988). It develops through recrystallisation of clay minerals into fine-grained mica minerals which align themselves normal to maximum stress, resulting in well-developed fissility, clearly visible in hand specimen.

Fig. 2. Hand specimen of carbonaceous phyllite, host rock of Mochia-Magra Pb-Zn Mines. The silky and satiny sheen luster with strong fissility is a diagnostic feature of phyllite, a low- to medium-grade metamorphic rock. The rock exhibits parallel alignment of very fine-grained platy minerals with shiny surface.

The mineralized rock was prepared as a polished thin section on a glass slide and studied microscopically under transmitted and reflected polarized light. Petrographic study in plane polarized light transmitted approach clearly distinguishes pyrite crystals with black color present in white colored carbonate-silicate matrix (Fig. 3a). Under cross polars, lamellar twinning is observed which is characteristic of calcite. Hence, the carbonate phase is calcite. Calcite grain displays very high order interference color. The grey color quartz grain exhibits undulatory extinction. Chlorite grains display platy texture having blue-green interference colors. Pyrite crystals remain opaque (Fig. 3b). Under plane polarized reflected light, pyrite is observed as bright yellow crystals embedded in greyish black calcite-silicate matrix (Fig. 3c). At 50X magnification, pyrite grains appear as euhedral to subhedral crystals, typically cubic in habit, showing sharp crystal boundaries, scattered throughout the matrix (Fig. 4a). Quartz appears as colorless grain with low relief. The carbonates are having higher relief with respect to quartz (Fig. 4b). The characteristic ore mineral assemblage (Fig. 4c), pyrite in association with quartz and calcite is indicative of hydrothermal fluid activities, where pyrite is crystalized first followed by quartz and calcite.

IV. THEORY AND METHODOLOGY

The petrographic study using a polarizing microscope involves examining rock and mineral over polished thin sections with polarized light to identify minerals, analyse rock textures, and determine their geological origin and evolution. The petrographic microscope uses polarizers and analysers to reveal birefringence and unique optical properties of minerals, converting them into visible colours and contrast. By observing these properties under various conditions such as plane-polarized, cross-polarized and reflected light mode. Petrographic studies offer advance detailed insights into a rock's mineralogical composition, microstructural characteristics, and evolutionary history.

The LRMS, uses an excitation laser is focused through an aperture on a Near-field Scanning Optical Microscopy (SNOM) tip on polished thin sections of carbonaceous phyllite sample. This creates an evanescent field (a non-propagating electromagnetic field) at the tip's apex. As the polished thin sections sample moves beneath the tip on a piezo-driven stage, the evanescent field interacts with the sample's surface. Raman scattered light from the illuminated spot is detected spectroscopically and processed point-by-point and line-by-line. The Laser Raman Scanning and 3D Mapping of polished thin section of carbonaceous sample were obtained at AFM Microscope with Raman-SNOM System situated in the Central Discovery Centre (CDC), Banaras Hindu University located in Varanasi, Uttar Pradesh, India (Pandit, 2024). The collected Raman spectra are used to generate hyperspectral images, which reveal the chemical composition and structure of the sample at the nanoscale. Achieves lateral resolutions of below 100 nm and Raman spectral resolution with an approximate ±3 cm^{-1} accuracy at room temperature relative to the internal standard, providing unprecedented detail compared to conventional Raman microscopy (Ferraro et al., 2003). Provides detailed chemical information from the Raman spectra, identifying specific molecules and materials. Acquires both chemical and topographical information simultaneously, RRUFF database offers a comprehensive support to analyzed samples in this study (Lafuente et al., 2015).

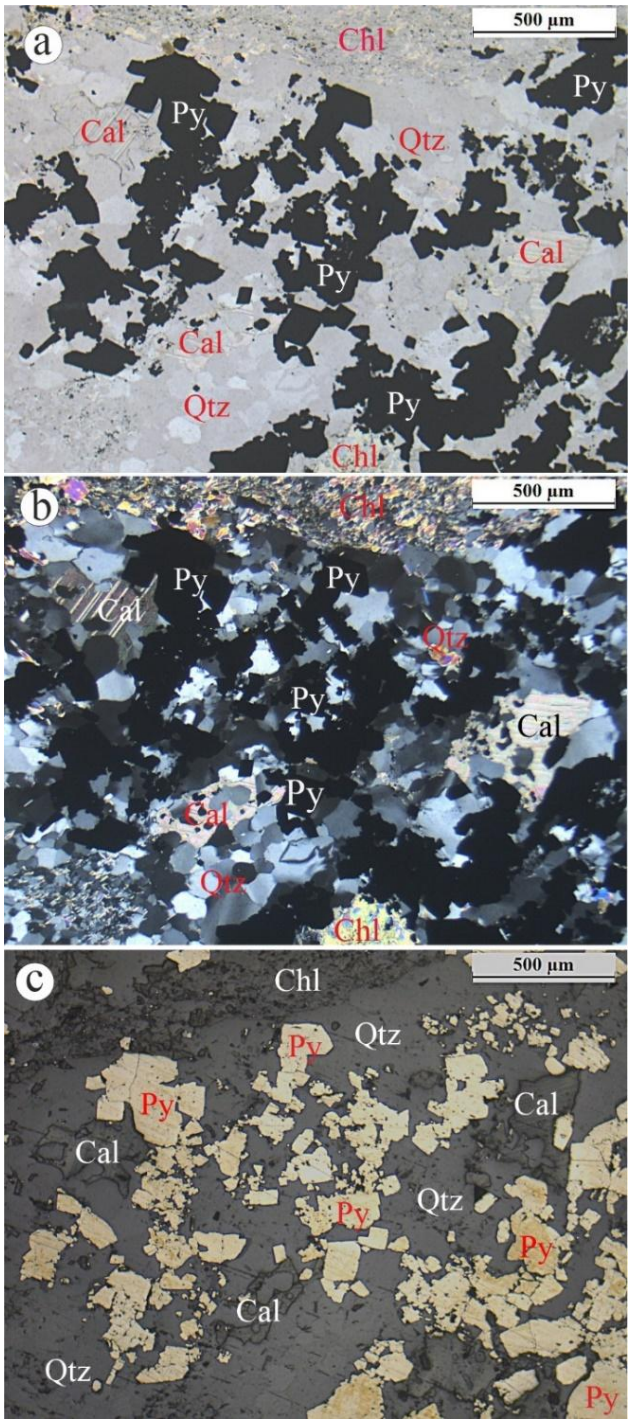

Fig. 3. Photomicrograph of carbonaceous phyllite from the Mochia-Magra Mines, Zawar Pb-Zn deposit in Udaipur district of Rajasthan. (a) Quartz-carbonate matrix is shown as colourless where carbonate exhibits slightly higher relief than quartz. Chlorite is pale greenish, low relief. Pyrite appears as black under plane polarized transmitted light mode. (b) Calcite shows lamellar or polysynthetic twinning and chlorite exhibits blue-green platy textures under cross polarised light mode. (c) Pyrite is seen as bright yellow crystals in quartz-carbonate matrix which is grey under reflected light mode. Abbreviations: Py - pyrite, Cal - calcite, Qtz - quartz, Chl – chlorite.

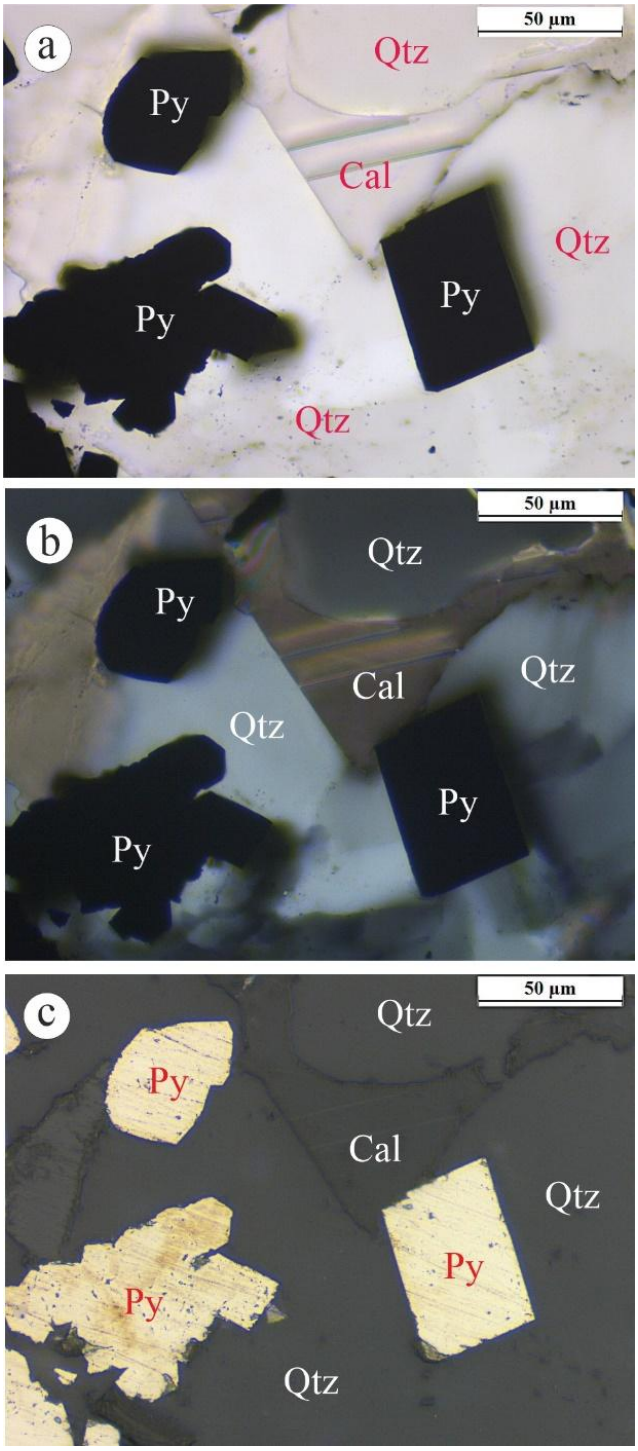

Fig. 4. Photomicrograph of carbonaceous phyllite from the Mochia-Magra Mines, Zawar Pb-Zn deposit, Udaipur, Rajasthan: (a) Pyrite appears as opaque with euhedral shape crystals, (b) Quartz exhibits undulatory extinction and polysynthetic twinning is observed in calcite crystals under crossed polarised light. (c) Pyrite appears as bright yellowish euhedral crystals that of typical cubic habit having high reflectance under reflected light mode. Abbreviations: Py - pyrite, Cal - calcite, Qtz - quartz, Chl - chlorite.

V. RESULTS

The Raman spectra were obtained over the pyrite, quartz and calcite crystal (Fig. 5a) deploying a laser beam from the Nd:YAG solid state device with 532 nm wavelength involved with the Microscope System Laser Raman-SNOM operating between output power of 0.3 To 1 mW (Singh and Pandit, 2025). The Raman-SNOM resolution can range from 2 to 4 cm^{-1} for routine tasks, with typical instruments offering a full spectral range from 100 to 3500 cm^{-1} in the MakeWITec, GmbH, Model: alpha 300-RAS devices with an accuracy of ±5cm^{-1} or even higher.

The bright yellow colour, euhedral pyrite (FeS_2) crystal is recognized with three representative Raman Bands at nearly 349, 383, and 438 cm^{-1} with respect to symmetry Tg(1) mode, Ag mode and Tg(3) mode, respectively (Fig. 5b). In pyrite crystal, the Raman Band or Shift ~349 cm^{-1} is attributed to degenerate Tg(1) mode and the Raman Band or Shift ~438 cm^{-1} is attributed to degenerate Tg(3) mode, whereas Raman Shift ~383 cm^{-1} is ascribed to totally symmetric Ag vibrational mode (Zhang et al., 2022). The Tg(1) and Tg(3) vibration mode correspond to a grouping of vibration and stretch movement, whereas Ag mode represent out of phase S-S stretching vibration (Sourisseau et al., 1991).

The quartz rich silicate matrix with grey colour (SiO_2) is categorized by three indicative Raman Bands at nearly 128, 206, and 466 cm^{-1} (Fig. 5c). The Raman Band or Shift at ~128 cm^{-1} of quartz is ascribed to the doubly degenerate E mode vibration while Raman Band or Shift at ~206 cm^{-1} favor Raman active mode A1 vibration (Li et al., 2025). The most intense Raman Band or Shift at ~466 cm^{-1} of quartz is developed because of four membered rings crystal structure of SiO_4-tetrahedra framework produce symmetric stretching vibration (Gillet et al., 1990).

The grey colour calcite crystal ($CaCO_3$) is recognized with the help of six indicative Raman bands or peaks at nearly 176, 299, 726, 1098, 1443, and 1757 cm^{-1} intensities (Fig. 5d). The Raman Band or Shift ~176 cm^{-1} and ~299 cm^{-1} in calcite is external vibration mode of $(CO_3)^{2-}$ group due to Mg cation substituting (Gunasekaran et al., 2006). The Raman Band or Shift ~726 cm^{-1} of calcite is attributed to symmetric deformation of $(CO_3)^{2-}$ group and ascribed to fundamental internal lattice vibration mode (Sun et al., 2014). The Raman Band or Shift ~1098 cm^{-1} of calcite is attributed to symmetrical stretching (v_1) vibration mode of the $(CO_3)^{2-}$ group (Gunasekaran and Anbalagan, 2007). The Raman Shift ~1443 and ~1757 cm^{-1} in calcite is attributed to asymmetric stretching (v_3) vibration mode of the $(CO_3)^{2-}$ group (Gunasekaran and Anbalagan, 2008).

The Raman Band or Shift at ~383 cm^{-1} of pyrite and Raman Band or Shift at ~466 cm^{-1} of quartz are applied to analyzed modes of vibration in mineral phases of the carbonaceous phyllite. The Raman Shift ~383 cm^{-1} of pyrite, corresponds to the in-phase stretching vibration of the S-S (disulfide) dumbbells within the crystal structure. Pyrite also has Eg (librational motion) and Tg (stretching and librational motions) modes that also provide information about its crystal structure, however, their intensities is relatively weak in this study (Zhang et al., 2022).

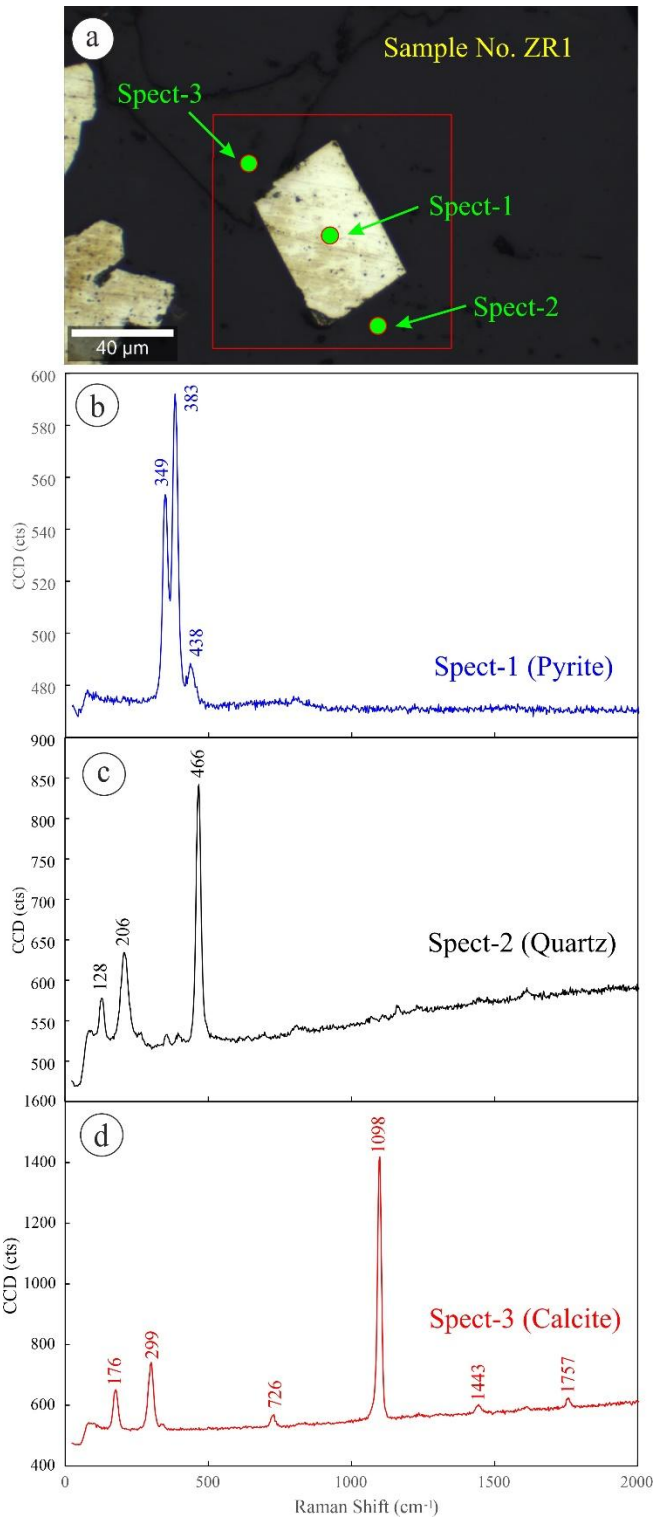

Fig. 5. (a) Representative photomicrograph shows pyrite crystal in the carbonaceous phyllite. Characteristic Raman spectra of (b) pyrite, (c) quartz, and (d) calcite crystals in the carbonaceous phyllite sample from the Mochia-Magra Pb-Zn Mines, Zawar in Udaipur district of Rajasthan.

The Raman Shift at ~466 cm^{-1} in quartz is a principal, symmetric, Si-O stretching mode that serves as a representative peak for quartz identification (Liu et al., 1997). The Si-O stretching mode is a fundamental vibration that can appear alongside other characteristics Raman Shift, such as those at approximately ~206 and ~128 cm^{-1}, and its intensity can be affected by processes of Fermi resonance (Watkins et al., 1990). Fermi resonance is an interaction in molecular vibrational spectroscopy where a fundamental vibrational transition mixes with an overtone or combination Raman Shift of the same symmetry that has a nearly identical energy (Monecke, 1987). This interaction causes the energy levels of the involved vibrations to shift and repel each other, splitting the bands in the spectrum and altering their intensities.

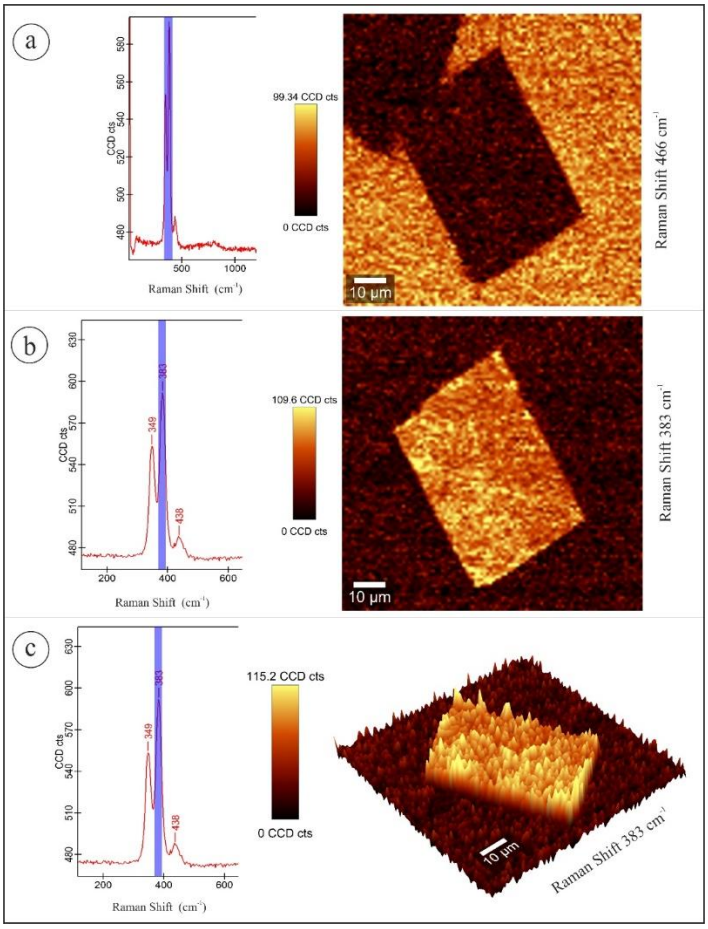

Fig. 6. Laser Raman scanning and mapping using SNOM of various mineral phases in carbonaceous phyllite from the Mochia-Magra Pb-Zn Mines. (a) Representative Raman spectrum of quartz matrix with 2D map of Raman Band or Shift at 466 cm^{-1}, (b) Raman spectrum of pyrite crystal with 2D map of Raman Band or Shift at 383 cm^{-1}, and (c) Raman spectrum scanning with 3D map of Raman Band or Shift at 383 cm^{-1} of pyrite crystal with euhedral shape.

In this study, diagnostic Raman Shift selected for pyrite (~383 cm^{-1}) and quartz (~383 cm^{-1}) is used to scanning the molecular structure of crystal in the carbonaceous phyllite using the Laser Raman SNOM instrument with 2D and 3D mapping. Euhedral pyrite crystal is perfectly grown surrounded by quartz and calcite crystal inside the carbonaceous phyllite (Fig. 6a). In 2D laser Raman mapping, the euhedral pyrite crystals display well-defined geometric rectangular shapes (Fig. 6b). In 3D laser Raman mapping, pyrite crystals can have smooth or striated faces, with the striations running parallel to crystallographic directions and sometimes featuring distinct macroscopic patterns called cubic surfaces (Fig. 6c). The presence and type of euhedral pyrite can provide insights into the geochemical conditions and formation mechanisms within sedimentary environments. While the outer shape is perfect, the internal structure or composition is not uniform that means an inhomogeneous euhedral pyrite crystal (Fig. 6c), which may contain variations in its chemical composition or trace element distribution. This means that as the crystal grew, the surrounding fluids or conditions changed, introducing different elements or altering the proportions of existing ones. The inhomogeneous distribution of elements points to dynamic changes in the geochemical environment during the crystal growth.

VI. DISCUSSIONS

Pyrite crystals occurred in the Zawar lead-zinc deposits, appearing in different forms and are found within carbonaceous phyllite, a foliated metamorphic rock containing fine-grained mica and carbonaceous material. In this study, pyrite crystal forms in association with carbonates (like calcite) and silicates (like quartz and clays) in the Machia-Magra mines. Pyrite crystal growth depends on conditions like sulphur supersaturation, temperature, and the presence of inhibitors or catalytic factors.

Pyrite crystal growth is a phase transition where atoms, ions, or molecules arrange themselves into a regular, repeating lattice structure, starting with nucleation (the formation of a seed crystal) and followed by growth of the nucleus into a larger crystal (Vekilov, 2010). Molecules or ions spontaneously come together to form tiny, stable clusters called nuclei or seeds. The overall process is driven by supersaturation, where the concentration of the species in a liquid or gas exceeds its solubility limit, spontaneous formation of stable nuclei, leading to their precipitation and ordering into the solid phase (Kalikmanov, 2013). From this stable nucleus, the crystal grows by the continuous addition of more atoms or molecules from the solution to its surface. The pyrite crystallization process begins with an iron-rich liquid solution, such as a hydrothermal fluid, when the solution becomes supersaturated, the excess iron and sulphur ions begin to precipitate out of the solution in the form of pyrite crystals (Chen et al., 2006). The specific growth conditions, such as temperature and pressure, and the concentration of sulphur, can influence the growth rate of pyrite (FeS_2) crystal faces, leading to different forms like cubes, dodecahedrons, or other perfect euhedral shapes (Pokrovski et al., 2021).

However, inhomogeneous pyrite crystal growth in the carbonaceous phyllite from Machia-Magra mines (Fig. 6c), refers to non-uniform development of pyrite (FeS_2) crystals due to varying environmental conditions, such as fluctuations in iron (Fe^{2+}) and sulphur (SO_4^{2-} or H_2S) concentrations, which influence supersaturation levels and surface energy dynamics (Wang and Morse, 1996; Karamova et al., 2025). Other environmental factors, such as cooling rate, the acidity of the fluids, and the overall concentration of dissolved elements (iron and sulphur), may also play a vital role in determining the exact shape of the pyrite crystal.

Conclusions

Pyrite, quartz, and calcite frequently occur together in the Mochia-Magra mines of the Zawar deposit, where they arise through fractures and weak surface planes in carbonaceous phyllite. Frequently, euhedral pyrite crystals are found in the carbonate-silicate matrix is specifies a well-known cubic form of pyrite (FeS_2), which is embedded within a phyllite host rock. In this study, Laser Raman scanning, 2D and 3D mapping of euhedral pyrite crystal infer their inhomogeneous composition in the carbonaceous phyllite. Origin of euhedral pyrite crystals, characterized by their perfect geometric forms like cubes and octahedrons, grow slowly from iron-sulphur rich hydrothermal solutions, often in a low-reactive iron environment or a diffusion-limited diagenetic zone. Pyrite crystallization within a carbonate-silicate association can occur in diverse geological settings, such as in carbonate-rich solution formed by methane-oxidizing and sulphate-reducing processes or during hydrothermal fluid activities. This combination suggests specific geological conditions, possibly hydrothermal fluids that influenced chemical precipitation processes, which lead to the crystallization of euhedral pyrite crystal within carbonaceous phyllite in the Zawar deposits. Investigations on the inhomogeneities in pyrite crystal benefits towards understand the complex geological processes of mineral formation, changes in physicochemical environment and the genesis of the ore deposits.

Acknowledgments

The authors acknowledged to the Head of the Department, Department of Geology, Institute of Science, Banaras Hindu University (BHU) for providing necessary facilities. AG acknowledged BHU sponsored Research Fellowship. DP acknowledged financial support from BHU-IoE sponsored SEED Grant and BHU-IoE sponsored Professional Development Fund (PDF).

References

Aradi, L.E., Spranitz, T., Myovela, J.L., Guzmics, T., Patko, L., & Berkesi, M. (2023) 3D Raman mapping combined with FIB-SEM on multiphase fluid inclusions: a tool to unravel complex phase assemblages. Journal of Raman Spectroscopy, 54, 1341-1352. https://doi.org/10.1002/jrs.6564.

Bersani, D. & Lottici, P.P. (2016) Raman spectroscopy of minerals and mineral pigments in archaeometry. Journal of Raman Spectroscopy, 47, 499-530. https://doi.org/10.1002/jrs.4914.

Bhattacharya, H.N. & Bull, S. (2010) Tectono-sedimentary setting of the Paleoproterozoic Zawar Pb–Zn deposits, Rajasthan, India. Precambrian Research, 177, 323–338. https://doi.org/10.1016/j.precamres.2010.01.004.

Biswal, T.K., Pradhan, R.M., Sharma, N.K., Tiwari, S.K., Beniest, A., Behera, B.H., Singh, S., Saraswati, R., Bhardwaj, A., Umasankar, B.H., Singh, Y.K., Sarkar, S., Mahadani, T. & Saha, G. (2022) A review on deformation structures of different terranes in the Precambrian Aravalli-Delhi Mobile Belt (ADMB), NW India: Tectonic implications and global correlation. Earth-Science Reviews, 230, 104037. https://doi.org/10.1016/j.earscirev.2022.104037.

Chakrabarti, A.K. (1967) Genesis of the lead-zinc deposits at Zawar, Rajasthan, India. Economic Geology, 62, 554-556. https://doi.org/10.2113/gsecongeo.62.4.554.

Chakrabarty, A.K. (1968) Cross-folding in the Zawar area, Rajasthan, India. Geological Society of America Bulletin, 79, 1677-1682. https://doi.org/10.1130/0016-7606(1968)79[1677:CITZAR]2.0.CO;2.

Chen, D.F., Feng, D., Su, Z., Song, Z.G., Chen, G.Q. & Cathles III, L.M. (2006) Pyrite crystallization in seep carbonates at gas vent and hydrate site. Materials Science and Engineering C, 26, 602-605. https://doi.org/10.1016/j.msec.2005.08.037.

Deb, M. & Sarkar, S.C. (1990) Proterozoic tectonic evolution and metallogenesis in the Aravalli-Delhi orogenic complex, northwestern India. Precambrian Research, 46, 115–137. https://doi.org/10.1016/0301-9268(90)90069-3.

Eberhardt, K., Stiebing, C., Matthaus, C., Schmitt, M. & Popp, J. (2015) Advantages and limitations of Raman spectroscopy for molecular diagnostics: an update. Expert Review of Molecular Diagnostics, 15, 773-787. https://doi.org/10.1586/14737159.2015.1036744.

Fareeduddin, & Banerjee, D.M. (2020) Aravalli Craton and its Mobile Belts: An Update. Episodes, 43, 88-108. https://doi.org/10.18814/epiiugs/2020/020005.

Ferraro, J.R., Nakamoto, K. & Brown, C.W. (2003). Introductory Raman Spectroscopy. Academic Press, San Diego, CA., pp 1-434. https://doi.org/10.1016/B978-0-12-254105-6.X5000-8.

Gillet, P., Cleach, A.L. & Madon, M. (1990) High-temperature Raman Spectroscopy of SiO_2 and GeO_2 polymorphs: anharmonicity and thermodynamic properties at high temperature. Journal of Geophysical Research: Solid Earth, 95, 21635-21655. https://doi.org/10.1029/JB095iB13p21635.

Gunasekaran, S. & Anbalagan, G. (2007) Spectroscopic characterization of natural calcite minerals. Spectrochimica

Acta Part A: Molecular and Biomolecular Spectroscopy, 68, 656-664. https://doi.org/10.1016/j.saa.2006.12.043.

Gunasekaran, S. & Anbalagan, G. (2008) Spectroscopic study of phase transitions in natural calcite mineral. Spectrochimica Acta Part A: Molecular and Biomolecular Spectroscopy, 69, 1246-1251. https://doi.org/10.1016/j.saa.2007.06.036.

Gunasekaran, S., Anbalagan, G. & Pandi, S. (2006) Raman and infrared spectra of carbonates of calcite structure. Journal of Raman Spectroscopy, 37, 892-899. https://doi.org/10.1002/jrs.1518.

Jones, R.R., Hooper, D.C., Zhang, L., Wolverson, D., & Valev, V.K. (2019) Raman Techniques: Fundamentals and Frontiers. Nanoscale Research Letters, 14, 231. https://doi.org/10.1186/s11671-019-3039-2.

Kalikmanov, V.I. (2013) Nucleation Theory. Lecture Notes in Physics, 860, XV, pp 1-319. https://doi.org/10.1007/978-90-481-3643-8.

Karamova, A., Karamov, T. & Spasennykh, M. (2025) Pyrite morphologies in Bazhenov Formation source rocks: diversity, systematic classification, sulfur isotopic composition and insights into sedimentation and diagenesis processes. Marine and Petroleum Geology, 182, 107535. https://doi.org/10.1016/j.marpetgeo.2025.107535.

Kosek, F., Nemec, I., Jehlicka, J. (2023) Raman study of several Cu-bearing complex minerals from the guano deposit at Pabellon de Pica, Tarapaca region, Chile. Journal of Raman Spectroscopy, 54, 1172-1182. https://doi.org/10.1002/jrs.6506.

Lafuente, B., Downs, R.T., Yang, H., & Stone, N. (2015) The power of databases: the RRUFF project. In: Highlights in Mineralogical Crystallography, T Armbruster & R M Danisi, eds. Berlin, pp 1-30.

Li, J., Chou, I.M., Wang, X., Liu, Y., Han, Z. & Gao, J. (2025) Pressure sensor based on the Raman shift of the 128 cm^{-1} band of quartz for pressure measurements in hydrothermal diamond-anvil cells. Chemical Geology, 674, 122558. https://doi.org/10.1016/j.chemgeo.2024.122558.

Liu, L., Mernagh, T.P. & Hibberson, W.O. (1997) Raman spectra of high-pressure polymorphs of SiO_2 at various temperatures. Physics and Chemistry of Minerals, 24, 396-402. https://doi.org/10.1007/s002690050053.

McMillan, P.F. (1989) Raman spectroscopy in mineralogy and geochemistry. Annual Review of Earth and Planetary Sciences, 17, 255-283. https://doi.org/10.1146/annurev.ea.17.050189.001351.

Misra, P.S., Pandit, D. and Saini, P. (2023) Raman Microspectrometry of fluid inclusions from quartz veins of eastern Mahakoshal belt, Central India. Journal of Scientific Research, 67, 11-17. http://dx.doi.org/10.37398/JSR.2023.670202.

Monecke, J. (1987) Theory of Fermi Resonances in Raman and Infrared spectra. Journal of Raman Spectroscopy, 18, 477-479. https://doi.org/10.1002/jrs.1250180705.

Mookherjee, A. (1964) The geology of the Zawar lead-zinc mine, Rajasthan, India. Economic Geology, 59, 656-677. https://doi.org/10.2113/gsecongeo.59.4.656.

Mookherjee, A. (1965) Regional structural framework of the lead-zinc deposits at Zawar, Rajasthan, India. Journal Geological Society of India, 6, 67-80. https://doi.org/10.17491/jgsi/1965/060111.

Nasdala, L. & Schmidt, C. (2020) Applications of Raman spectroscopy in mineralogy and geochemistry. Elements, 16(2), 99-104. https://doi.org/10.2138/gselements.16.2.99.

Pandit, D. (2024) Characterization of Sulphide Ore Minerals Using Combined Laser Raman with Scanning Near-field Optical Microscopy (SNOM). Journal of Scientific Research, 68(3), 1-5. http://dx.doi.org/10.37398/JSR.2024.680301.

Pokrovski, G.S., Blanchard, M., Saunier, G. & Poitrasson, F. (2021) Mechanisms and rates of pyrite formation from hydrothermal fluid revealed by iron isotopes. Geochimica et Cosmochimica Acta, 304, 281-304. https://doi.org/10.1016/j.gca.2021.03.006.

Power, K.B. & Patwardhan, A.M. (1984) Tectonic evolution and base-metal mineralisation in the Aravalli-Delhi Belt, India. Precambrian Research, 25, 309-323. https://doi.org/10.1016/0301-9268(84)90038-X.

Ramakrishnan, M. & Vaidyanadhan, R. (2008) Geology of India (Volume 1 & 2). Geological society of India, Bangalore.

Raman, C.V. & Krishnan, K.S. (1928) A new type of secondary radiation. Nature, 121, 501-502. https://doi.org/10.1038/121501c0.

Raman, C.V. (1923) The scattering of light by liquid and solid surfaces. Nature, 112, 281-282. https://doi.org/10.1038/112281a0.

Raman, C.V. (1928) A new radiation. Indian Journal of Physics, 2, 387-398. http://dspace.rri.res.in/handle/2289/2135.

Raman, C.V. (1929) The Raman effect: investigation of molecular structure by light scattering. Transactions of the Faraday Society, 25, 781-792. https://doi.org/10.1039/TF9292500781.

Robinson, J.W., Roberts, W.W. & Matzger, A.J. (2024) Kidney stone growth through the lens of Raman mapping. Scientific Reports, 14, 10834. https://doi.org/10.1038/s41598-024-61652-9.

Rodgers, K.A. (1993) Routine identification of aluminum hydroxide polymorphs with the Laser Raman Microscope. Clay Minerals, 28, 85-99. https://doi.org/10.1180/claymin.1993.028.1.08.

Roy, A.B. & Purohit, R. (2015) Lithostratigraphic, geochronological and depositional framework of the Precambrian basins of the Aravalli Mountains and adjoining areas, Rajasthan, India. In: Mazumder, R. & Eriksson, P. G. (eds) 2015. Precambrian Basins of India: Stratigraphic and

Tectonic Context. Geological Society, London, Memoirs, 43, 55-65, http://dx.doi.org/10.1144/M43.4.

Roy, A.B. (1990) Evolution of the Precambrian crust of the Aravalli Mountain range. In: S.M. Naqvi (ed.), Precambrian Continental Crust and its Economic Resources, Development in Precambrian Geology, Elsevier, pp 327-348. https://doi.org/10.1016/S0166-2635(08)70173-7.

Roy, A.B. (1995) Geometry and Evolution of Superposed Folding in the Zawar Lead–Zinc mineralized belt, Rajasthan. In: Proceedings, Indian Academy of Sciences, Earth & Planetary Science, 104, 349–371.

Sarkar, S.C. & Banerjee, S. (2004) Carbonated-hosted Lead-Zinc deposits of Zawar, Rajasthan, in the Context of world scenario. In: Sediment Hosted Lead-Zinc Sulphide Deposits, Eds M. Deb and W.D. Goodfellow, W.D., pp 1-328.

Sharma, R.S. (2009) Cratons and fold belts of India. Springer, pp 1-304. https://doi.org/10.1007/978-3-642-01459-8.

Sharma, S.K., Misra, A.K., Lucey, P.G. & Lentz, R.C.F. (2009) A combined remote Raman and LIBS instrument for characterizing minerals with 532 nm laser excitation. Spectrochimica Acta, Part A 73, 468-476. https://doi.org/10.1016/j.saa.2008.08.005.

Singh, A.K. and Pandit, D. (2025) Petrography and Laser Raman Characterization of Banded Hematite Jasper from Agori Formation of Mahakoshal Greenstone Belt. Journal of Scientific Research, 69, 1-7. http://dx.doi.org/10.37398/JSR.2025.690201.

Singh, N.N. (1988) Tectonic and stratigraphic framework of the lead-zinc sulphide mineralisation at Zawarmala, district Udaipur, Rajasthan. Journal Geological Society of India. 31, 546-564. https://doi.org/10.17491/jgsi/1988/310603.

Sourisseau, C., Cavagnat, R., & Fouassier, M. (1991) The vibrational properties and valence force fields of FeS_2, RuS_2 pyrites and FeS_2 marcasite. Journal of Physics and Chemistry of Solids, 52, 537-544. https://doi.org/10.1016/0022-3697(91)90188-6.

Sun, J., Wu, Z., Cheng, H., Zhang, Z. & Frost, R.L. (2014) A Raman spectroscopic comparison of calcite and dolomite. Spectrochimica Acta Part A: Molecular and Biomolecular Spectroscopy, 117, 158-162. http://dx.doi.org/10.1016/j.saa.2013.08.014.

Talluri, J.K., Pandalai, H.S. & Jadhav, G.N. (2000) Fluid Chemistry and Depositional Mechanism of the Epigenetic, Discordant Ores of the Proterozoic, Carbonate-Hosted, Zawarmala Pb-Zn Deposit, Udaipur District, India. Economic Geology, 95, 1505-1525. https://doi.org/10.2113/gsecongeo.95.7.1505.

Vandenabeele, P. (2013) Practical Raman Spectroscopy - An Introduction. John Wiley & Sons, Ltd. DOI:10.1002/9781119961284.

Vekilov, P.G. (2010) Nucleation. Crystal Growth & Design, 10, 5007-5019. https://doi.org/10.1021/cg1011633.

Verma, P.K. & Greiling, R.O. (1995) Tectonic evolution of the Aravalli orogen (NW India): an inverted Proterozoic rift basin? Geologische Rundschau, 84, 683-696. https://doi.org/10.1007/BF00240560.

Wang, Q. & Morse, J.W. (1996) Pyrite formation under conditions approximating those in anoxic sediments I. Pathway and morphology. Marine Chemistry, 52, 99-121. https://doi.org/10.1016/0304-4203(95)00082-8.

Watkins, G.D., Fowler, W.B., Stavola, M., DeLeo, G.G., Kozuch, D.M., Pearton, S.J. & Lopata, J. (1990) Identification of a Fermi Resonance for a defect in silicon: deuterium-boron pair. Physical Review Letters, 64, 467-470. https://doi.org/10.1103/PhysRevLett.64.467.

Zhang, H., Qian, G., Cai, Y., Gibson, C. & Pring, A. (2022) Crystal chemistry of arsenian pyrites: A Raman spectroscopic study. American Mineralogist, 107, 274-281. https://doi.org/10.2138/am-2021-7806.

*****